DOI: 10.1002/chem.200700808

Large-Scale Synthesis of Single-Crystalline RE_2O_3 (RE = Y, Dy, Ho, Er) Nanobelts by a Solid–Liquid-Phase Chemical Route

Min Han,[a, b] Nai-En Shi,[a] Wen-Li Zhang,[a] Bao-Jun Li,[a] Jian-Hua Sun,[a] Kun-Ji Chen,[b] Jian-Ming Zhu,[b] Xin Wang,[c] and Zheng Xu*[a]

Abstract: Yttrium-group heavy rare-earth sesquioxide (RE_2O_3, RE = Y, Dy, Ho, Er) nanobelts were successfully fabricated by thermolysis of solid RE-$(NO_3)_3{\cdot}x\,H_2O$ in a dodecylamine/1-octadecene mixed solvent system. The synthetic principle is based on separating the nucleation and growth processes by utilizing the poor solubility of $RE(NO_3)_3{\cdot}\chi\,H_2O$ in the solvent mixture and the heat-transportation difference between the liquid and solid. By using dodecylamine, RE_2O_3 nanobelts can be readily obtained. X-ray diffraction (XRD) analysis shows that the synthesized RE_2O_3 nanobelts are body-centered cubic and crystalline. Field-emission scanning electron microscopy (FE-SEM), transmission electron microscopy (TEM), selective-area electron diffraction (SAED), and high-resolution transmission electron microscopy (HR-TEM) demonstrate that the synthesized RE_2O_3 compounds possess regular geometric structure (beltlike) with perfect crystallinity. Preliminary experimental results prove that the dodecylamine plays a key role in the formation of RE_2O_3 nanobelts and cannot be replaced by other surfactants. Furthermore, this method can be extended to the synthesis of RE_2O_3 nanobelt/metal nanocrystal nanocomposites and ABO_3 (A = Y, Dy, Ho, Er; B = Al) and $A_3B_5O_{12}$ (A = Y, Dy, Ho, Er; B = Al)-type ternary oxide nanobelts, using mixed-metal nitrate salts in the correct stoichiometry instead of single rare-earth nitrates.

Keywords: crystal growth · crystal nucleation · nanobelts · rare earths · solid–liquid phase

Introduction

The development and innovation of synthetic strategies for materials is of great importance in the advancement of science and technology. Thermal decomposition based on non-hydrolytic systems or a combination method (i.e., organometallic precursors in high-boiling-point organic solvents are decomposed or combined to obtain the desired inorganic nanocrystals) has proven to be highly versatile and reliable. Using this method, many highly monodispersed metal[1–3] and semiconductor nanocrystals[4–6] with tuneable sizes and shapes have been successfully synthesized. However, the shapes of the obtained nanocrystals are mainly spherical, cubic, rodlike, arrowlike, multipod-like, and polyhedral.[7–11] The quasi-1D beltlike nanostructure (i.e., the nanobelt), which was discovered in 2001[12] and serves as an ideal candidate material for studying the fundamental physical and chemical properties in confined systems,[13,14] has not been effectively and systematically synthesized by using this method. To the best of our knowledge, only CdSe nanoribbons have been synthesized by using the reaction of $CdCl_2$ and octylammonium selenocarbamate in an octylamine media very recently.[15] Therefore, exploring and developing

[a] Dr. M. Han, Dr. N.-E. Shi, Dr. W.-L. Zhang, B.-J. Li, J.-H. Sun, Prof. Z. Xu
State Key Laboratory of Coordination Chemistry
School of Chemistry and Chemical Engineering
Nanjing University, Nanjing 210093 (China)
Fax: (+86) 25-8331-4502
E-mail: zhengxu@netra.nju.edu.cn

[b] Dr. M. Han, Prof. K.-J. Chen, Prof. J.-M. Zhu
National Laboratory of Solid State Microstructures Department of Physics, Nanjing University
Nanjing 210093 (China)

[c] Prof. X. Wang
Laboratory of Material Chemistry
School of Chemistry and Chemical Engineering, Nanjing University of Science and Technology
Nanjing 210093 (China)

Supporting information for this article is available on the WWW under http://www.chemeurj.org/ or from the author. It contains TEM images of the Y_2O_3 samples synthesized under different conditions; HR-TEM and SAED patterns of the Dy_2O_3, Ho_2O_3 and Er_2O_3 nanobelts; and TEM images of the Y_2O_3 nanobelts loaded with silver nanocrystals from using a mixed nitrate salt instead of single rare earth nitrates.

a nonhydrolytic thermal synthetic method to fabricate other functional nanobelts on a large scale is necessary and continues to be a key challenge in the field of material synthesis.

As a class of important functional materials, rare-earth sesquioxides (RE_2O_3) have attracted much attention because these materials have potential applications in many industrial fields.[16] Some methods, such as solvothermal and thermal decomposition, have been used to synthesize RE_2O_3 nanoparticles, nanowires, nanodisks, and nanotubes.[11,17–21] Recently, light rare-earth sesquioxide (La_2O_3) nanobelts were synthesized through a mixed alkali/solvent method combined with thermal treatment.[22] However, yttrium-group heavy rare-earth sesquioxide (RE_2O_3, RE = Y, Dy, Ho, Er) nanobelts have not been reported so far, which may be attributed to their extremely high melting points (m.p. $\approx$2500 °C). Therefore, it is necessary to search for an effective method to synthesize RE_2O_3 (RE = Y, Dy, Ho, Er) nanobelts which is not only important for fundamental research but also for application in practical fields.

Herein, we report a nonhydrolytic thermal decomposition route to synthesize RE_2O_3 (RE = Y, Dy, Ho, Er) single-crystalline nanobelts. The typical synthesis is based on the thermolysis of solid $RE(NO_3)_3{\cdot}xH_2O$ (RE = Y, Dy, Ho, Er) in a dodecylamine/1-octadecene mixed solvent from room temperature to 320 °C at a rate of 6 °C min^{-1}. Because the starting materials are solid and have poor solubility in the organic liquid media, we refer to this process as a "solid–liquid-phase chemical route". Taking advantage of the poor solubility of $RE(NO_3)_3{\cdot}xH_2O$ in these solvents, and the difference in heat transportation between the liquid and solid, the nucleation and growth processes can be efficiently separated, which is different from the conventional "hot-injection" method.[4,23,24] The operation is quite simple and environmentally friendly, with no release of NO_x pollutants. Also, this method is effective for the synthesis of single-crystalline RE_2O_3 (RE = Y, Dy, Ho, Er) nanobelts on a gram scale. We use Y_2O_3 nanobelts as a typical example for discussion of the experimental results; the other nanobelts will be briefly introduced.

Results and Discussion

XRD analysis of the Y_2O_3 nanobelts: The phase structure and crystallinity of the Y_2O_3 nanobelts was examined by X-ray diffraction (XRD) studies (Figure 1). Ten obvious diffraction peaks were observed. In comparison with the Joint Committee on Powder Diffraction Standard Card (JCPDS) No. 82–2415, those peaks can be indexed as (211), (222), (400), (332), (134), (440), (611), (622), (444), and (662) planes of the body-centered cubic phase Y_2O_3. The result shows that the product has good crystallinity.

FE-SEM, TEM, and HR-TEM analysis of the Y_2O_3 nanobelts: Typical field-emission scanning electron microscopy (FE-SEM) images of the Y_2O_3 nanobelts are shown in Figure 2. A low-magnification FE-SEM image (Figure 2a) shows large-surface-area straight and bent beltlike nanostructures, which are several micrometers in length. A representative high-magnification SEM image (Figure 2b) reveals that each nanobelt has a uniform width of about 50–220 nm and a thickness of about 20–30 nm along the entire length. The ratio of width to thickness is about 2–10:1. The rectangular cross sections of the nanobelts also can be observed (the regions indicated by the arrows in Figure 2b). The small particles on the surface of the belts are attributed to the sputtered gold nanoparticles during the FE-SEM measurements.

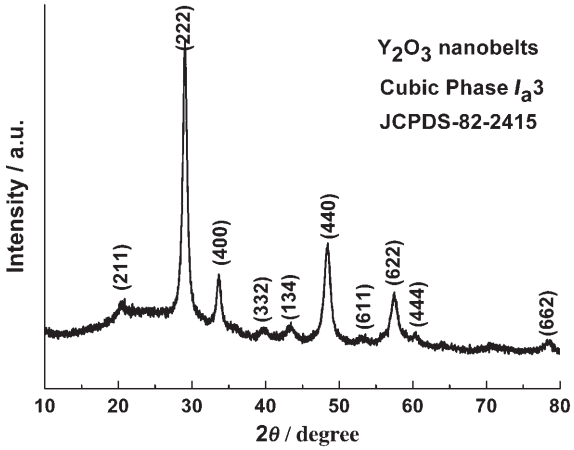

Figure 1. XRD pattern of the synthesized Y_2O_3 nanobelts.

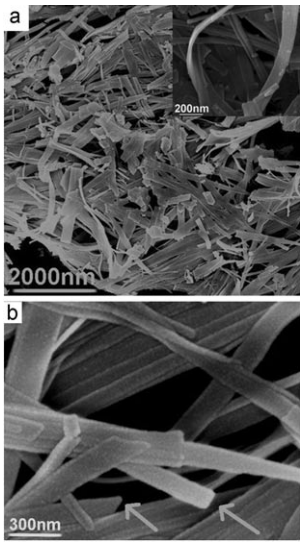

Figure 2. FE-SEM images of the synthesized Y_2O_3 nanobelts. a) Low-magnification FE-SEM image, inset shows the bent nanobelts. b) High-magnification FE-SEM image.

Transmission electron microscopy (TEM) observation (Figure 3a) demonstrates that the as-synthesized Y_2O_3 possesses beltlike structures, which is consistent with the FE-

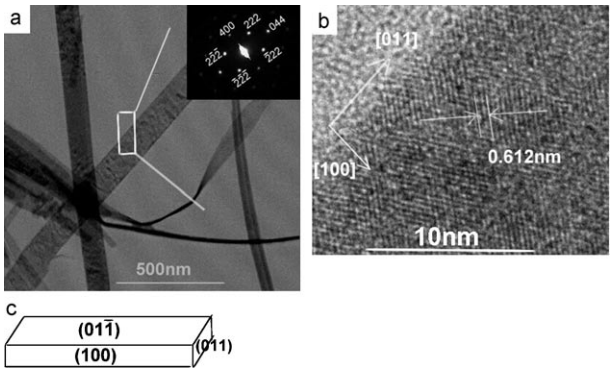

Figure 3. TEM images of the synthesized Y_2O_3 sample. a) Low-magnification TEM image of the Y_2O_3 nanobelts. b) HR-TEM image of a single Y_2O_3 nanobelt. c) Schematic diagrams of the geometrical configuration of the Y_2O_3 nanobelt.

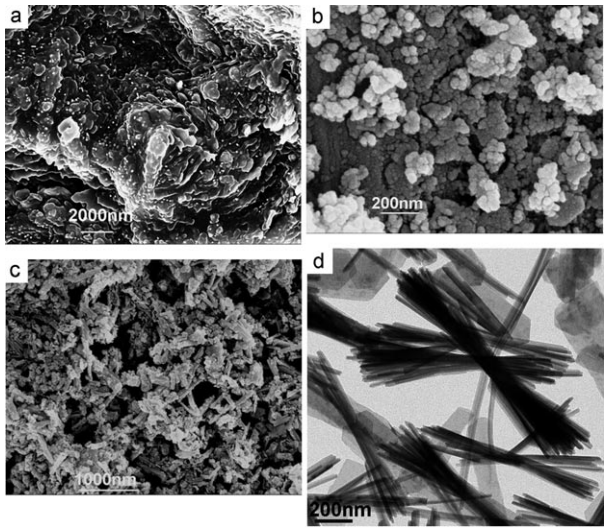

Figure 4. FE-SEM images and TEM image of the Y_2O_3 sample synthesized using various surfactants instead of dodecylamine while keeping other conditions constant. a) CTAB, b) SDS, c) OA, d) TEM image of the synthesized Y_2O_3 nanobelts using hexadecylamine instead of dodecylamine.

SEM result. A selected-area electron diffraction (SAED) pattern (inset of Figure 3a) recorded perpendicular to the top surface of the nanobelt shows clear diffraction spots along the entire length of the nanobelt, thus indicating that the nanobelt is structurally uniform and singularly crystalline. The corresponding zone axis is [01$\bar{1}$], thus suggesting that the thickness direction of the nanobelt is (01$\bar{1}$). A high-resolution TEM (HR-TEM; Figure 3b) image shows clear fringes and gives lattice spacing of 3.06 Å, which corresponds to the interplanar separation between the (222) plane of the body-centered cubic phase of Y_2O_3. Taken together the SAED and HRTEM results shows that the preferred growth direction (or long axis) of the Y_2O_3 nanobelt is (011) and the width direction (or side surface) is (100). A related schematic pattern is shown in Figure 3c.

Growth mechanism of the Y_2O_3 nanobelts: Because the starting material is solid yttrium nitrate and the solvent is a mixture of 1-octadecene and dodecylamine, we speculate that the formation of Y_2O_3 nanobelts follows a "solid–liquid–solid" (SLS) process, which may be as follows: In the initial stage, a small amount of solid nitrate is gradually dissolved in the solvent to form an intermediate complex with the dodecylamine as the temperature increases. The dissolved nitrate decomposes to form the crystal nuclei. With a further increase in temperature, the decomposition reaction begins to take place violently at the interface between the solid surface and solvent. Subsequently, the decomposed product enters into the liquid phase with the help of the dodecylamine, which leads to the growth of the crystal nuclei. The color of the liquid phase turns to light brown concomitantly as a result of the by-product NO_x, which reacts with dodecylamine and 1-octadecene. As a result of the efficient separation of nucleation from growth, 1D nanostructures may be obtained. Dodecylamine plays a key role in the formation of 1D beltlike nanostructures and cannot be replaced by other surfactants, such as cetyltrimethylammonium bromide (CTAB), sodium dodecylsulfate (SDS), and oleic acid (OA; Figure 4a–c). Although Y_2O_3 nanobelts can be obtained using hexadecylamine instead of dodecylamine, the nanobelts form bundles and the size distribution becomes broad (Figure 4d). The reason for this behavior may be that increasing the chain length of the organoamine leads to greater steric barriers and Van der Waals interactions, which affect the growth dynamic process and the aggregation of the organoamines. In addition, the temperature of the solvent at which the solid starting material is added has a great impact on the morphology of the obtained product. High-quality Y_2O_3 nanobelts are obtained when the solvent containing the solid starting material is heated from room temperature to 320 °C; whereas only sheetlike microstructures with two sharp tips and some nanoparticles are obtained when the starting material is added directly at 320 °C (see the Supporting Information).

To obtain further insight into the growth mechanism of the Y_2O_3 nanobelts, their growth process was studied by monitoring the reaction at different temperatures and with different ripening times. When the reaction temperature reached 200 and 262 °C, two samples were extracted and their morphologies were evaluated by TEM analysis (see the Supporting Information). When the reaction temperature reached 200 °C, the short beltlike nanostructures appeared with some spherical nanoparticles. When the temperature reached 262 °C, the spherical nanoparticles disappeared and only the beltlike nanostructures remained. This behavior may give a hint to the formation mechanism of the nanobelts, namely, that nanobelts are likely to grow from those nanoparticles. After the reaction temperature reached 320 °C, another four samples were taken at 4, 10, 20, and 30 min (samples 1–4, respectively); the corresponding TEM images are shown in Figure 5. When the reaction temperature was kept at 320 °C for 4 min (sample 1), large-surface-

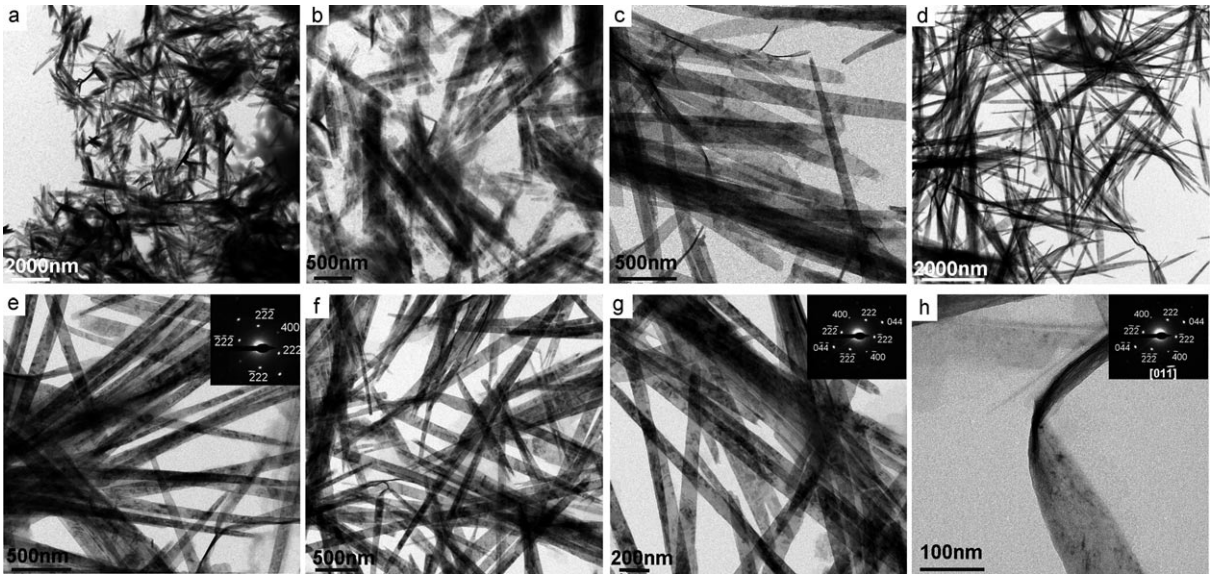

Figure 5. TEM images of the synthesized Y_2O_3 nanobelts treated at 320 °C for different times. TEM images of sample 1 after incubation for 4 min at a) low- and b) high-magnification. c) TEM image of sample 2 after incubation for 10 min. d,e) TEM images of sample 3 after incubation for 20 min. The inset of (e) shows the corresponding SAED pattern for an individual nanobelt. f–h) The corresponding TEM images of sample 4 after incubation for 30 min. The insets of (g) and (h) are the SAED patterns for the individual straight and bent nanobelts.

area nanobelts were observed (Figure 5a,b) with a length and width of about 1.0–2.0 μm and 55–200 nm, respectively. However, the crystallinity of the nanobelts was poor. Only concentric rings appeared in the SAED pattern. With the increasing reaction time, the nanobelts continued to grow. For sample 2 (10 min), the length and width of the nanobelts reached approximately 3 μm and 60–220 nm (Figure 5c). For sample 3 (20 min), the length of the nanobelts reached approximately 5–10 μm (Figure 5d,e). SAED analysis along the entire length of the nanobelts showed clear diffraction spots, thus confirming the formation of single-crystalline Y_2O_3 nanobelts. On further prolonging of the reaction time, the crystallinity and quality of the nanobelts was much higher. High-quality straight and twisted nanobelts were obtained when the reaction temperature was kept at 320 °C for 30 min (Figure 5f–h). As the reaction system involves solid and liquid phases, the nucleation and growth process are quite complicated. Therefore, the detailed formation mechanism cannot be given at present and further study is needed.

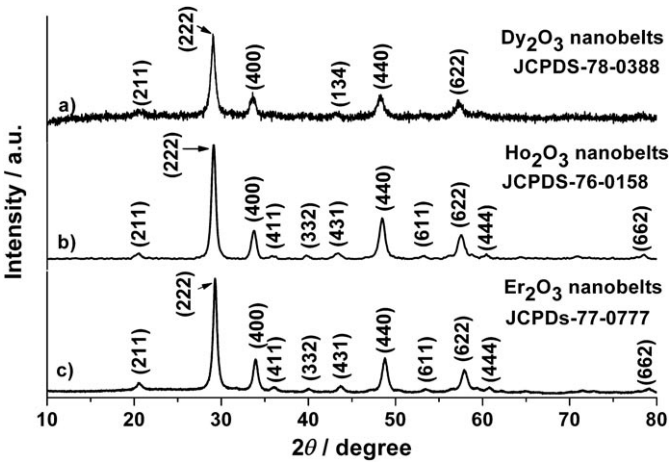

Figure 6. XRD pattern of the synthesized Dy_2O_3 (a), Ho_2O_3 (b), and Er_2O_3 (c) nanobelts.

Synthesis and analysis of Dy_2O_3, Ho_2O_3, and Er_2O_3 nanobelts: Keeping the volumes of dodecylamine and 1-octadecene constant, Dy_2O_3, Ho_2O_3, and Er_2O_3 nanobelts can be obtained by using solid $Dy(NO_3)_3{\cdot}x\,H_2O$, $Ho(NO_3)_3{\cdot}x\,H_2O$, and $Er(NO_3)_3{\cdot}x\,H_2O$, respectively, instead of solid $Y(NO_3)_3{\cdot}6\,H_2O$. The XRD patterns of the Dy_2O_3, Ho_2O_3, and Er_2O_3 nanobelts are shown in Figure 6 and typical FE-SEM and TEM images in Figure 7. The length of the Dy_2O_3, Ho_2O_3, and Er_2O_3 nanobelts is about several micrometers, their widths are about 30–250 nm, and their thicknesses are about 15–60 nm. The ratio of width to thickness is about 2–15:1. Corresponding SAED and HRTEM analysis (see the Supporting Information) demonstrates that all the nanobelts are highly crystalline and are consistent with the XRD results. From a series of experiments, we found that the formation of rare-earth sesquioxide nanobelts is correlated to the structural nature of the oxides. The present experimental results demonstrate that by using this method yttrium-group heavy rare-earth sesquioxides readily form nanobelts, whereas light rare-earth sesquioxide nanobelts are difficult to obtain by the same procedure. In addition, it should be mentioned that RE_2O_3 nanobelts loaded with silver nanocrystals (see the Supporting Information) can be easily obtained by using $AgNO_3$ and solid $RE(NO_3)_3$ instead of just solid $RE(NO_3)_3$. The experimental results show that RE_2O_3 nanobelts loaded with silver nanocrystals are excellent cata-

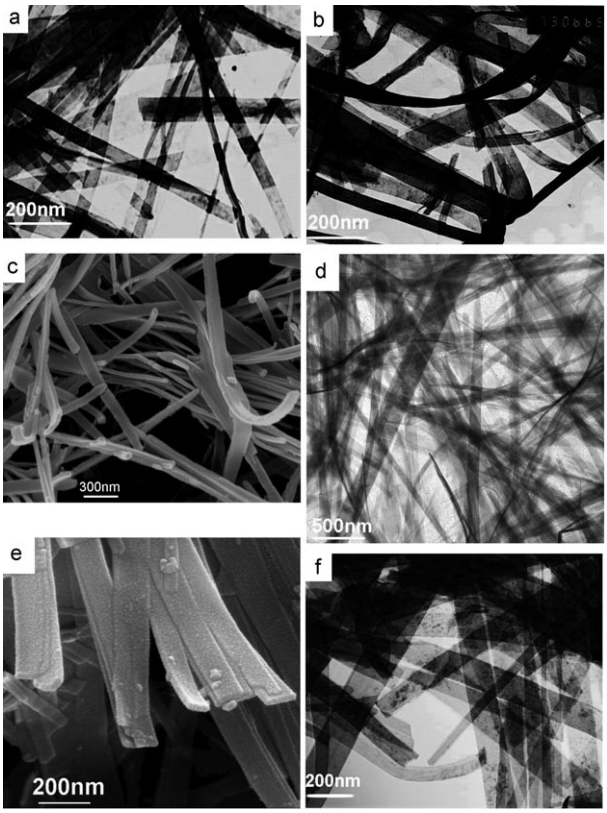

Figure 7. TEM and FE-SEM images of the synthesized RE_2O_3 sample. a), b) TEM images of the Dy_2O_3 nanobelts. c, d) FE-SEM and TEM images of the Ho_2O_3 nanobelts, respectively. e, f) FE-SEM and TEM images of the Er_2O_3 nanobelts, respectively.

lysts for the hydrogenation of nitro compounds in high yield and selectivity, which will be reported later.

Conclusion

In summary, by using a facile solid–liquid-phase chemical route RE_2O_3 (RE = Y, Dy, Ho, Er) single-crystalline nanobelts with body-centered cubic phase structures have been successfully synthesized on a gram scale under low-temperature and atmospheric-pressure conditions. The remarkable features of this method are that a common $RE(NO_3)_3{\cdot}\chi H_2O$ solid is used as the starting material, and a single surfactant (i.e., dodecylamine) serves as the capping reagent. The process is simple, economic, and environmental friendly. Furthermore, this method can be extended to synthesize RE_2O_3 nanobelt/metal nanocrystal nanocomposites and ABO_3-(A = Y, Dy, Ho, Er; B = Al) and $A_3B_5O_{12}$ (A = Y, Dy, Ho, Er; B = Al)-type ternary oxide nanobelts, by using mixed metal nitrate salts in stoichiometric proportions instead of a single rare earth nitrate. This development not only enriches the present family of nanobelts but also provides new opportunities to fabricate nanobelt-based functional devices. Further study on the growth mechanism of nanobelts through our system will promote the development of nucleation and growth theory in a heterogeneous-phase system.

Experimental Section

Chemicals: All chemicals used in this study are analytical-grade reagents obtained commercially without further purification. The chemical reagents were rare earth nitrate salts ($RE(NO_3)_3{\cdot}xH_2O$, purity > 99.9%, Shanghai), heptane, absolute alcohol (analytical grade, Shanghai), dodecylamine (> 98.0%, Aldrich), and 1-octadecene (technical grade, > 90%, Aldrich).

Typical synthesis of Y_2O_3 nanobelts: A solid sample of $Y(NO_3)_3{\cdot}6H_2O$ (1.05–4.50 g), dodecylamine (10–20 mL), and 1-octadecene (5–10 mL) were added to a 250-mL three-necked flask. Subsequently, the reactor was heated to 320 °C at a rate of 6 °C min^{-1} and maintained at 320 °C for 30 min. A crude product was obtained, which could be dispersed in nonpolar solvents. Addition of absolute ethanol (50 mL) caused the formation of a white precipitate, which was separated and washed with heptane and absolute ethanol several times to remove the by-products. Finally, the precipitate was dried in vacuum at 60 °C for 4 h. The dried precipitate was calcinated in air at 500 °C for 2 h at a heating rate of 1.5 °C min^{-1}. The organic compounds covering the surface of the nanobelts were readily removed, which did not destroy the shape of the product.

Synthesis of Dy_2O_3, Ho_2O_3, and Er_2O_3 nanobelts: The synthetic processes were similar to that for the Y_2O_3 nanobelts. Solid samples of $Dy(NO_3)_3{\cdot}xH_2O$, $Ho(NO_3)_3{\cdot}xH_2O$, and $Er(NO_3)_3{\cdot}xH_2O$ were used instead of solid $Y(NO_3)_3{\cdot}6H_2O$, and the other conditions were kept constant, thus easily obtaining Dy_2O_3, Ho_2O_3, and Er_2O_3 nanobelts. The post-treatment processes were the same as for Y_2O_3 nanobelts.

Characterization: The XRD patterns were recorded on a powder sample using an X'Pert diffractometer (Panalytical) with $Cu_{K\alpha}$ radiation (λ = 1.5406 Å) in 2θ ranging from 10 to 80°. The corresponding work voltage and current was 40 kV and 40 mA, respectively. FE-SEM images were taken on a LEO-1530 VP scanning-electron microscope with an accelerating voltage of 20 kV. The TEM images were taken on a JEM-200CX instrument (Japan) with an accelerating voltage of 200 kV. The HR-TEM images were recorded on a JEOL-2010 apparatus at an accelerating voltage of 400 kV.

Acknowledgements

We thank Prof. Shuyuan Zhang (University of Science and Technology of China, Structure Research Laboratory, Hefei, Anhui 230026, China) for help with HR-TEM characterization and analysis. This study was supported by the National Natural Science Foundation of China (NSFC) under major project nos. 90606005 and 20490210, and project nos. 20571040 and 20371026.

[1] a) S. Sun, C. B. Murray, D. Weller, L. Folks, A. Moser, *Science* **2000**, *287*, 1989–1992; b) H. Zeng, J. Li, J. P. Liu, Z. L. Wang, S. H. Sun, *Nature* **2002**, *420*, 395–398.

[2] V. F. Puntes, K. M. Krishnan, A. P. Alivisatos, *Science* **2001**, *291*, 2115–2117.

[3] a) F. Dumestre, B. Chaudret, C. Amiens, P. Renaud, P. Fejes, *Science* **2004**, *303*, 821–823; b) D. Kim, J. Park, K. An, N. K. Yang, J. G. Park, T. Hyeon, *J. Am. Chem. Soc.* **2007**, *129*, 5812–5813.

[4] a) A. L. Rogach, D. V. Talapin, H. Weller, in *Colloids and Colloid Assemblies, Chapter 2* (Eds.: Frank Caruso), Wiley-VCH, Weinheim, **2004**, pp. 52–94; b) C. D. Donega, P. Liljeroth, D. Vanmaekelbergh, *Small* **2005**, *1*, 1152–1162.

[5] a) J. E. Murphy, M. C. Beard, A. G. Norman, S. P. Ahrenkiel, J. C. Johnson, P. Yu, O. I. Micic, R. J. Ellingson, A. J. Nozik, *J. Am. Chem. Soc.* **2006**, *128*, 3241–3242; b) M. V. Kovalenko, E. Kaufmann, D. Pachinger, J. Roither, M. Huber, J. Stang, G. Hesser, F. Schaffler, W. Heiss, *J. Am. Chem. Soc.* **2006**, *128*, 3516–3517.

[6] a) S. H. Choi, E. G. Kim, T. Hyeon, *J. Am. Chem. Soc.* **2006**, *128*, 2520–2521; b) C. H. Lee, M. Kim, T. Kim, A. Kim, J. Paek, J. W.

Lee, S. Y. Choi, K. Kim, J. B. Park, K. Lee, *J. Am. Chem. Soc.* **2006**, *128*, 9326–9327.

[7] a) J. Joo, H. B. Na, T. Yu, J. H. Yu, Y. W. Kim, F. Wu, J. Z. Zhang, T. Hyeon, *J. Am. Chem. Soc.* **2003**, *125*, 11100–11105; b) J. Park, K. An, Y. Hwang, J. G. Park. , H. J. Noh, J. Y. Kim, J. H. Park, N. M. Hwang, T. Hyeon, *Nat. Mater.* **2004**, *3*, 891–895; c) T. Yu, J. Joo, Y. I. Park, T. Hyeon, *Angew. Chem.* **2005**, *117*, 2577–7580; *Angew. Chem. Int. Ed.* **2005**, *44*, 7411–7414.

[8] a) X. Peng, L. Manna, W. Yang, J. Wickham, E. Scher, A. Kadavanich, A. P. Alivisatos, *Nature* **2000**, *404*, 59–61; b) L. Manna, E. C. Scher, A. P. Alivisatos, *J. Am. Chem. Soc.* **2000**, *122*, 12700–12706; c) Z. A. Peng, X. Peng, *J. Am. Chem. Soc.* **2002**, *124*, 3343–3353; d) A. G. Kanaras, C. Sonnichsen, H. Liu, A. P. Alivisatos, *Nano Lett.* **2005**, *5*, 2164–2167.

[9] a) Y. W. Jun, S. M. Lee, N. J. Kang, J. Cheon, *J. Am. Chem. Soc.* **2001**, *123*, 5150–5151; b) A. B. Panda, G. Glaspell, M. S. EI-Shall, *J. Am. Chem. Soc.* **2006**, *128*, 2790–2791.

[10] a) M. Ghosh, K. Biswas, A. Sundaresan, C. N. R. Rao, *J. Mater. Chem.* **2006**, *16*, 106–111; b) K. Biswas, C. N. R. Rao, *J. Phys. Chem. B* **2006**, *110*, 842–845; c) M. Ghosh, E. V. Sampathkumaran, C. N. R. Rao, *Chem. Mater.* **2005**, *17*, 2348–2352; d) K. Sardar, C. N. R. Rao, *Adv. Mater.* **2004**, *16*, 425–429.

[11] R. Si, Y. W. Zhang, L. P. You, C. H. Yan, *Angew. Chem.* **2005**, *117*, 3320–3324; *Angew. Chem. Int. Ed.* **2005**, *44*, 3256–3260.

[12] a) Z. W. Pan, Z. R. Dai, Z. L. Wang, *Science* **2001**, *291*, 1947–1949; b) W. S. Shi, H. Y. Peng, N. Wang, C. P. Li, L. Xu, C. S. Lee, R. Kalish, S. T. Lee, *J. Am. Chem. Soc.* **2001**, *123*, 11095–11096.

[13] a) Z. L. Wang, *Annu. Rev. Phys. Chem.* **2004**, *55*, 159–196; b) A. Pan, H. Yang, R. Liu, R. Yu, B. Zuo, Z. L. Wang, *J. Am. Chem. Soc.* **2005**, *127*, 15692–15693; c) Y. K. Liu, J. A. Zapien, Y. Y. Shan, C. Y. Geng, C. S. Lee, S. T. Lee, *Adv. Mater.* **2005**, *17*, 1372–1377; d) Y. B. Li, Y. Bando, D. Golberg, K. Kurashima, *Appl. Phys. Lett.* **2002**, *81*, 5048–5050.

[14] a) Z. Liu, S. Li, Y. Yang, S. Peng, Z. Hu, Y. Qian, *Adv. Mater.* **2003**, *15*, 1946–1948; b) J. Zhang, J. Du, B. Han, Z. Liu, T. Jiang, Z. Zhang, *Angew. Chem.* **2006**, *118*, 1134–1137; *Angew. Chem. Int. Ed.* **2006**, *45*, 1116–1119.

[15] J. Joo, J. S. Son, S. G. Kwon, J. H. Yu, T. Hyeon, *J. Am. Chem. Soc.* **2006**, *128*, 5632–5633.

[16] G. X. Xu in *Rare earth*, Metallurgical Industry Press, Beijing, China, **1995**.

[17] T. Liu, Y. H. Zhang, H. Y. Shao, X. G. Li, *Langmuir* **2003**, *19*, 7569–7572.

[18] X. Wang, Y. D. Li, *Angew. Chem.* **2002**, *114*, 4984–4987; *Angew. Chem. Int. Ed.* **2002**, *41*, 4790–4793.

[19] a) X. Wang, X. M. Sun, D. P. Yu, B. S. Zou, Y. D. Li, *Adv. Mater.* **2003**, *15*, 1442–1445; b) A. W. Xu, Y. P. Fang, L. P. You, H. Q. Liu, *J. Am. Chem. Soc.* **2003**, *125*, 1494–1495; c) M. Yada, M. Mihara, S. Mouri, M. Kuroki, T. Kijima, *Adv. Mater.* **2002**, *14*, 309–312.

[20] a) G. S. Wu, L. D. Zhang, B. C. Cheng, T. Xie, X. Y. Yuan, *J. Am. Chem. Soc.* **2004**, *126*, 5976–5977; b) Y. P. Fang, A. W. Xu, L. P. You, R. Q. Song, J. C. Yu, H. X. Zhang, Q. Li, H. Q. Liu, *Adv. Func. Mater.* **2003**, *13*, 955–960.

[21] H. Wang, M. Uehara, H. Nakamura, M. Miyazaki, H. Maeda, *Adv. Mater.* **2005**, *17*, 2506–2509.

[22] C. G. Hu, H. Liu, W. T. Dong, Y. Y. Zhang, G. Bao, C. S. Lao, Z. L. Wang, *Adv. Mater.* **2007**, *19*, 470–474.

[23] C. B. Murray, D. J. Norris, M. G. Bawendi, *J. Am. Chem. Soc.* **1993**, *115*, 8706–8707.

[24] J. Park, E. Lee, N. M. Hwang, M. Kang, S. C. Kim, Y. Hwang, J. G. Park, H. J. Noh, J. Y. Kim, J. H. Park, T. Hyeon, *Angew. Chem.* **2005**, *117*, 2932–2937; *Angew. Chem. Int. Ed.* **2005**, *44*, 2872–2877.

Received: May 28, 2007
Revised: August 30, 2007
Published online: November 20, 2007

